

# NJC

Accepted Manuscript



This is an *Accepted Manuscript*, which has been through the Royal Society of Chemistry peer review process and has been accepted for publication.

*Accepted Manuscripts* are published online shortly after acceptance, before technical editing, formatting and proof reading. Using this free service, authors can make their results available to the community, in citable form, before we publish the edited article. We will replace this *Accepted Manuscript* with the edited and formatted *Advance Article* as soon as it is available.

You can find more information about *Accepted Manuscripts* in the [Information for Authors](#).

Please note that technical editing may introduce minor changes to the text and/or graphics, which may alter content. The journal's standard [Terms & Conditions](#) and the [Ethical guidelines](#) still apply. In no event shall the Royal Society of Chemistry be held responsible for any errors or omissions in this *Accepted Manuscript* or any consequences arising from the use of any information it contains.



[www.rsc.org/njc](http://www.rsc.org/njc)

## ARTICLE

## Facile synthesis of electrochemically active Pt nanoparticle decorated carbon nano onions

Cite this: DOI: 10.1039/x0xx00000x

Haibo Lu,<sup>a,b</sup> Paul K. Eggers,<sup>b,c</sup> Christopher T. Gibson,<sup>c</sup> Xiaofei Duan,<sup>d</sup> Robert N. Lamb,<sup>d</sup> Colin L. Raston<sup>c</sup> and Hui Tong Chua<sup>\*a</sup>,

Received 00th January 2014,  
Accepted 00th January 2014

DOI: 10.1039/x0xx00000x

www.rsc.org/

Well dispersed platinum nanoparticles 1-5 nm (average 2 nm) in diameter on carbon nano onions (CNOs) are accessible using a simple and scalable one-step batch method. This technique involves pre-treatment of acid digested CNOs with  $\text{H}_2\text{PtCl}_6$  prior to reduction using hydrogen at ambient conditions, with the composite material being electrochemically active. The effect of different Pt loading, surface treatment, and the processing temperature on the dispersion of platinum nanoparticles on the CNOs has been studied in detail.

### Introduction

Graphitic carbon substrates in the form of carbon nanotubes (CNTs),<sup>1</sup> carbon nanofibers (CNFs),<sup>2</sup> and graphene sheets<sup>3</sup> are highly conductive scaffolds with impressive mechanical and structural properties. Their large surface areas offer scope for dispersing noble metal nanoparticles with enhanced functionality. Indeed carbon-supported metal catalysts have promising electrochemical activity for application in chemical sensors<sup>4</sup> and fuel cells.<sup>5</sup>

Related to the above forms of carbon are the so called carbon nano onions (CNOs). The electrochemical performance of CNOs for potential use as supercapacitor electrodes has been studied and reviewed in detail.<sup>6</sup> Decorating them with metal nanoparticles has also attracted considerable attention in heterogeneous catalysis and for use in high capacity Li-ion batteries where there is excellent cycling performance.<sup>7</sup> Recently we demonstrated that CNOs can be produced with a low-cost large-scale methane cracking method,<sup>8</sup> thereby laying down the foundation for the industrial uptake of this unique carbon nanomaterial. Furthermore, a vortex fluidic device (VFD) has been shown to produce CNOs-Pd and CNOs-Pt nanocrystalline hybrid materials for sensor and fuel cell applications.<sup>9</sup> In previous work, plasma etching and *p*-phosphonic acid calix[8]arene had been used as surface modification strategies to disperse CNOs,<sup>9a,9b</sup> resulting in 2–7 nm Pd and ~20 nm Pt being deposited onto CNOs, depending on the speed of VFD.

In the present paper, in contrast with our earlier work,<sup>9</sup> the CNOs can be directly decorated by ~2 nm Pt nanoparticles with uniform distribution and high density using hydrogen as the reducing agent in a simple and passive setup, thereby obviating the use of any harsh surface modification of CNOs and any special high-speed device. The results establish a relatively cost

effective, benign and scalable batch process, auguring for easy adoption in standard industrial reactors. Raw CNOs were first treated with nitric acid to eliminate the encapsulated catalyst responsible for decomposing methane to carbon and hydrogen. Decoration thereafter with well distributed Pt nanoparticles of ~2 nm diameter was achieved using a simple and scalable one-step method, as shown in Fig. 1. This involves the use of hydrogen gas at ambient pressure as the reducing agent for  $\text{H}_2\text{PtCl}_6$  in a CNO suspension. Moreover, the use of hydrogen rather than ascorbic acid, avoids any preferential facet growth directed by the reducing agent and/or its oxidised form. In this study, the effects of the concentration of Pt-precursors, different CNO pre-treatment methods, and temperature were examined to demonstrate control over the size, morphology and dispersion of Pt nanoparticles decorated on the CNOs. Furthermore, we also demonstrate the significant electrocatalytic behaviour of the Pt-decorated CNOs, thereby providing an attractive prospect for application of the material in various industrial applications.

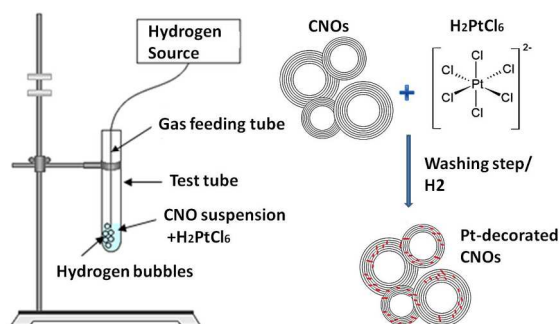


Fig. 1. Schematic of the Pt nanoparticles decoration on carbon nano-onions (CNOs).

## Experimental

### Materials

CNOs, which were synthesized by a methane cracking method,<sup>Error! Bookmark not defined.</sup> were initially suspended in concentrated nitric acid (HNO<sub>3</sub>) and ultrasonicated for 1 hour, followed by refluxing at 180 °C overnight to remove metallic impurities. The product was filtered, washed with Milli-Q water several times and then dried in an oven at 120 °C.

Aqueous solutions of hexachloroplatinic(IV) acid (H<sub>2</sub>PtCl<sub>6</sub>), HNO<sub>3</sub> and H<sub>2</sub>SO<sub>4</sub> and other reagents were of analytical grade and were used as received. All aqueous solutions were prepared with Milli-Q water.

### Preparation of Pt/CNOs composites

0.5, 1, 2, 5, 7, 10, and 15 μL of Pt precursor, as 0.1 mol/L H<sub>2</sub>PtCl<sub>6</sub> solution was dropped into 0.5 mL CNOs suspension solution with a concentration of 0.2 mg/mL. The solution was ultrasonicated for 5 min then aged for at least ~24 hours at room temperature. Excess Pt(IV) complex was removed by high-speed centrifugation (~16 900× g, 30 min) at room temperature. The resultant supernatant was withdrawn using a pipette, and then the sediment was re-dispersed in Milli-Q water, and centrifuged with this operation repeated three times. A suspension solution of CNOs-H<sub>2</sub>PtCl<sub>6</sub> was placed into a test tube, and hydrogen gas was purged into it for 10 min at room temperature, as shown in Fig. 1. The resulting solutions were centrifuged three times as above, to remove any residual Pt nanoparticles in solution. A successful scale-up decoration using the proposed method was also carried out with 12.5 mL (in contrast with 0.5 mL) CNOs suspension solution with a similar procedure as above, which augurs well for the further scalability of this decoration process.

The syntheses were carried out under the same experimental conditions using plasma-etched CNOs as the starting material for comparison. The plasma-etched CNOs were treated using a GaLa Instrument PlasmaPrep in ambient air.

### Characterization techniques

Scanning electron microscopy (SEM) measurements were carried out on a ZEISS 1555 VPSEM. Transmission electron microscopy (TEM) and high resolution TEM (HRTEM) measurements were conducted on a JEOL-2100 transmission electron microscope. The TEM samples were prepared by transferring one drop of the suspension on a 200 mesh carbon-coated copper TEM grid. Raman spectra were also acquired on CNO samples using a Witec alpha300R Raman microscope with excitation laser wavelength of 532 nm (≤ 5 mW). 20 to 30 single spectra were recorded with a x40 objective (Numerical Aperture 0.60) for each sample at approximately 5 separate locations within each sample. Typical integrations times were between 30 to 120 seconds for 2 to 3 accumulations per spectrum. XPS data were acquired using a VG ESCALAB220i-XL spectrometer equipped with a hemispherical analyser. The

incident radiation was monochromatic Al K $\alpha$  X-rays (1486.6 eV) at 220 W (22 mA and 10kV). Survey (wide) and high resolution (narrow) scans were taken at analyser pass energies of 100 eV. Survey scans were carried out over 1200-0 eV binding energy range with 1.0 eV step size and 100 ms dwell time. Narrow high resolution scans were run over 20 eV (or 40eV for Fe) binding energy range with 0.05 eV step size and 250 ms dwell time. Base pressure in the analysis chamber was below 7.0×10<sup>-9</sup> mbar. A low energy flood gun was used to compensate the surface charging effect. All data were processed using CasaXPS software.

### Electrochemical measurements

Electrochemical measurements were performed on a Gamry Reference 600 Potentiostat. A conventional three-electrode system was used including a Ag/AgCl reference electrode, a Pt wire as the counter electrode and the Pt/CNOs with various Pt amount as the working electrode. All the electrochemical data were reported versus Ag/AgCl. Glassy carbon (GC) disk electrodes (3 mm diameter) were employed, which were polished successively by aluminum oxide particles on cloth polishing pads and then washed in milli-Q water under ultrasonication. In order to prepare the working electrode, the Pt-decorated CNOs samples were centrifuged to a final higher concentration, and was placed onto a GC electrode, and dried under a lamp for 1 hour. 1.0 M H<sub>2</sub>SO<sub>4</sub> (Scharlau, 95-97% reagent grade) was used as the electrolytic solution. Cyclic voltammetry (CV) measurements of the work electrodes were performed in a potential range of -0.3 to 1.28 V (vs. Ag/AgCl) with scanning rate of 200 mV s<sup>-1</sup>.

## Results and discussion

After introducing hydrogen into the suspension solution of CNOs-H<sub>2</sub>PtCl<sub>6</sub> for 10 min at room temperature, the products in the test tube were centrifuged and collected. SEM and TEM were used to analyse the CNOs before and after decoration. As illustrated in Fig. 2a, raw CNOs from methane cracking are numerous quasi-spheres in the range of 50-200 nm in diameter encapsulating catalyst nanoparticles (Fig. 2a inset), with CNT as a minor side product. Complete removal of the catalyst and functionalization of the CNOs is accomplished through liquid-phase oxidation using concentrated nitric acid at 90 °C for 24 hours. The purified CNO exhibits a hollow onion-like structure, Fig. 2b. The lattice fringes in HRTEM image show the characteristics of graphitic carbon, in which a d-spacing of 0.34 nm (indicated by parallel lines) corresponds to the (002) plane spacing, Fig. 2c and inset. As shown in Fig. 2d, the CNOs were successfully decorated with a dense and uniform distribution of Pt nanoparticles, in contrast with the purified CNO, Fig. 2b. The HRTEM images, Fig. 2e, show that the Pt nanoparticles are quasispherical in shape with an average size of ~2 nm. As calculated from Fig. 2d, there is ~1 Pt nanoparticle per 100 nm<sup>2</sup> of CNOs, with an average surface area of about 13 nm<sup>2</sup> for each Pt nanoparticle. The lattice fringes of the Pt nanoparticles in Fig. 2e show a d-spacing of 0.23 nm (as indicated by parallel lines) which coincides with a face centred cubic (fcc) Pt(111).

The selected area electron diffraction (SAED) pattern, Fig. 2f, is consistent with the results of TEM analysis. The lattice parameters calculated from the SAED data also established that Pt nanoparticles had been decorated onto the CNOs.

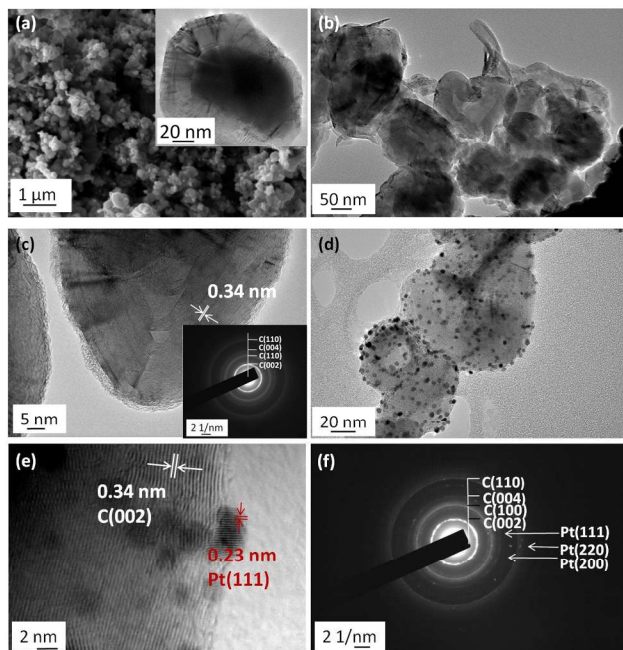


**Fig. 2** (a) SEM and TEM (inset) images of raw CNOs, (b-c) TEM and HRTEM images with SAED pattern (inset) of the purified CNOs, (d-f) TEM and HRTEM images, and SAED pattern of Pt-decorated CNOs with 0.1 M  $\text{H}_2\text{PtCl}_6$  precursor of 5  $\mu\text{L}$  added into the CNOs suspension.

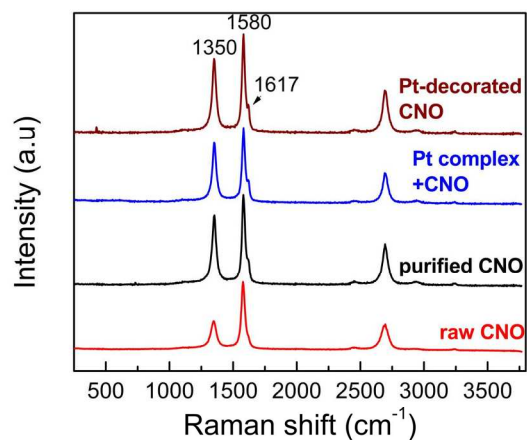


**Fig. 3** Raman spectra of raw and purified CNOs, and CNO- $\text{H}_2\text{PtCl}_6$  before and after  $\text{H}_2$  reduction.

Raman spectra, comparing as-prepared and purified CNOs, Fig. 3, consist of the D band near  $1350\text{ cm}^{-1}$  accompanied by a D' band at  $1617\text{ cm}^{-1}$  related to a disordered graphitic structure, and a G band at  $1580\text{ cm}^{-1}$  associated with a crystalline graphitic structure. The peaks at the higher regions ( $2300$  to  $3300\text{ cm}^{-1}$ ) are assigned to overtone and combinational

scattering of the G and D bands.<sup>10</sup> The G/D peak intensity ratio has been used to determine the relative degree of disordered carbon and other structural imperfections in CNOs.<sup>11</sup>

An average of the G/D ratios for each sample was calculated and displayed in Table 1. The G/D ratios for raw and purified CNOs were found to be 2.3 and 1.3, respectively, suggesting the highly graphitic nature of the samples. Purified CNOs manifests a number of functional groups due to the nitric acid treatment, such as hydroxyl, carboxyl and carbonyl groups.<sup>12</sup> The creation of functional groups produces defects (and therefore disorder) in the CNO structure and decreases the G/D peak intensity ratio. Moreover, the presence of oxygen on the surface coordinates the metal centres which on reduction, allows for the nucleation, growth and attachment of platinum nanoparticles.

**Table 1** G/D ratios from Raman test for each sample

Sample	G/D ratio	Error (1 standard deviation)
Raw CNOs	2.3	0.3
Purified CNOs	1.3	0.1
Purified CNOs with $\text{H}_2\text{PtCl}_6$ acid	1.2	0.1
Pt decorated CNOs	1.4	0.2

The control showed that CNOs cannot be decorated without using hydrogen, although as shown in Fig. 4a-b, a small amount of unattached agglomerated Pt nanoparticles were found. Moreover, the decoration procedure is easily scalable by increasing the initial amount of CNOs suspension and  $\text{H}_2\text{PtCl}_6$  solution, and the corresponding period of hydrogen reduction, as shown in Fig. 4c-d.

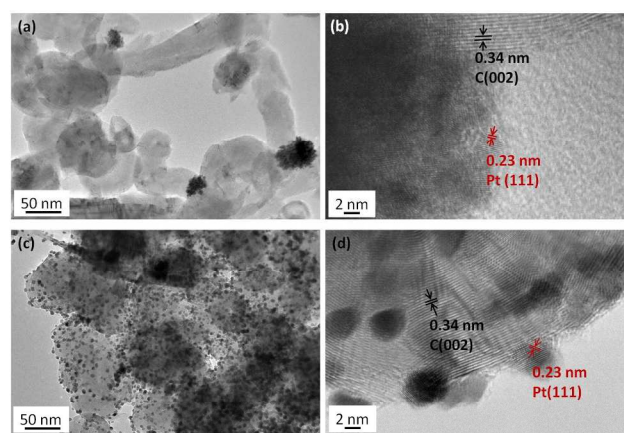


**Fig. 4.** TEM images of CNOs- $\text{H}_2\text{PtCl}_6$  (a-b) before and (c-d) after  $\text{H}_2$  reduction using a scale-up decoration procedure.

X-ray photoelectron spectroscopy (XPS) was used to characterize the raw, purified, CNOs- $\text{H}_2\text{PtCl}_6$  and its  $\text{H}_2$ -reduced products. The C1s and O1s peaks are present in all samples, Fig. 5a. However, the oxygen amount in the purified CNOs (4.97 at.%) was significantly higher on the surface of the CNOs as compared to the as-received raw CNOs (2.38 at.%); indicating surface oxidation by the acid treatment. After the addition of  $\text{H}_2\text{PtCl}_6$  into CNOs suspension, the expected Pt4f peaks were observed for the samples before and after  $\text{H}_2$  reduction. From the expanded Pt4f region, Fig. 5b, the oxidation states of the metal centres can be identified as Pt(II) and Pt(IV) prior to  $\text{H}_2$  reduction. After  $\text{H}_2$  reduction, the peaks ascribed to Pt(II) and Pt(IV) are dwarfed by a low energy band centred at 71.5 eV and a high energy band at 74.9 eV which indicate the presence of a significant amount of metallic Pt(0). XPS results established that the Pt amount before and after  $\text{H}_2$  reduction are 0.47 at% and 2.12 at%, respectively.

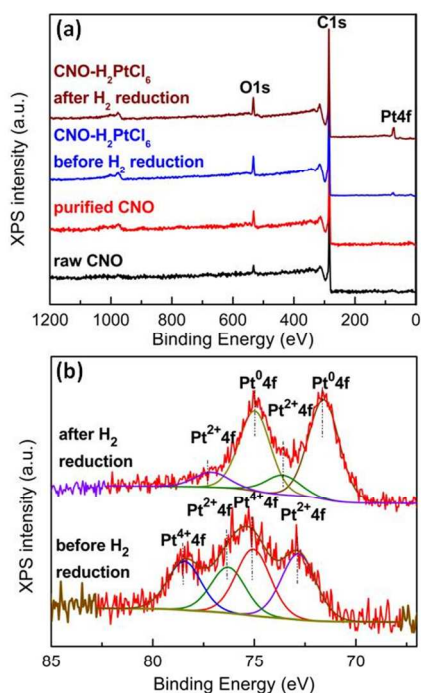


**Fig. 5.** XPS spectra of (a) the raw CNO, purified CNOs, CNOs- $\text{H}_2\text{PtCl}_6$  before and after  $\text{H}_2$  reduction, (b) the Pt4f region for the aforementioned samples.

Controlling the size, morphology and dispersion of noble metal nanoparticles on the various types of carbon supports has been a major challenge.<sup>13</sup> There are many parameters associated with the decoration procedure that affect the reduction process, the particle size and distribution. These include the choice of reducing agent, the use and nature of any surfactants, any pre-treatment processing of the carbon substrate, temperature and pH.<sup>9,13</sup>

In this investigation, the growth density of the Pt nanoparticles was controlled through adjusting the initial amount of Pt precursor added from 1, 2, 5, 7, 10 to 15  $\mu\text{L}$  as 0.1

mol/L  $\text{H}_2\text{PtCl}_6$  solution into 0.5 mL CNO suspension (0.2 mg/mL), Fig. 6. The concentration of  $\text{H}_2\text{PtCl}_6$  precursor in the CNO suspension was 0.2, 0.4, 1.0, 1.4, 2.0, and 3.0 mM, respectively. The metal loading of all the Pt-decorated CNOs is summarized in Table 2.

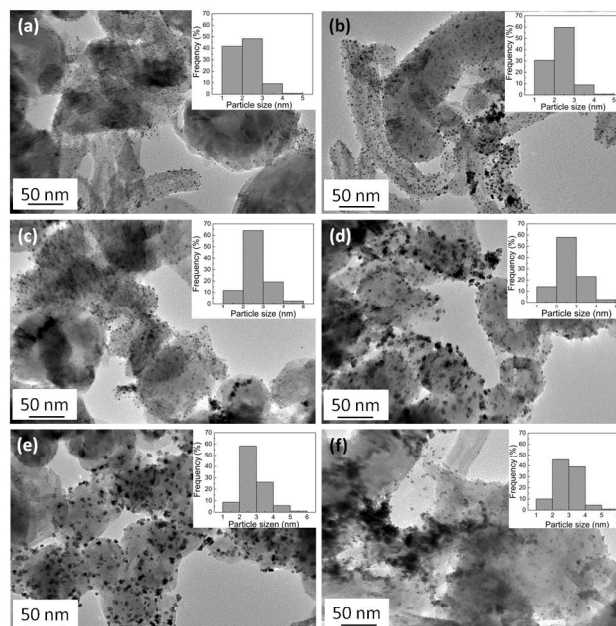


**Fig. 6.** TEM images of Pt@CNOs composites formed using 0.1 M  $\text{H}_2\text{PtCl}_6$  precursor of (a) 1  $\mu\text{L}$ , (b) 2  $\mu\text{L}$ , (c) 5  $\mu\text{L}$ , (d) 7  $\mu\text{L}$ , (e) 10  $\mu\text{L}$  and (f) 15  $\mu\text{L}$ .

**Table 2** Pt% for each sample in CNOs suspension

Volume of 0.1 mol/L $\text{H}_2\text{PtCl}_6$ ( $\mu\text{L}$ )	Mass of Pt (mg)	Pt loading of Pt/CNOs (wt %)
1	0.02	20
2	0.04	40
5	0.1	100
7	0.14	140
10	0.2	200
15	0.3	300

When 1  $\mu\text{L}$  of 0.1 mol/L  $\text{H}_2\text{PtCl}_6$  precursor was added into the CNO suspension, a low density of Pt particles resulted on the surface of CNOs, Fig. 6a. This suggests that the concentration of the Pt precursor was too low to decorate all CNOs. Increasing the amount of Pt precursor to 2.0, then 5.0  $\mu\text{L}$  revealed an increase in density of the decorated Pt nanoparticles, Fig. 6b and 6c, while maintaining the average

size of the Pt nanoparticles at approximately 2 nm. Pt nanoparticles with the average size of 4 nm increased when the amount of  $\text{H}_2\text{PtCl}_6$  added was greater than  $7.0 \mu\text{L}$ , as shown in particle size histograms, Fig. 6 inset. Moreover, at this concentration the Pt nanoparticles began to agglomerate, Fig. 6d. Once the amount of Pt precursor was increased to  $15 \mu\text{L}$ , very large agglomerates were evident, Fig. 6f. As shown in Fig. 2 and Fig 6, the uniform distribution and highest density of Pt particles resulted from 40 to 100 wt% Pt loading in the Pt-decorated CNOs, as shown in Table 2.

To study how temperature can change the size, morphology and decoration density of Pt nanoparticles, reactions were carried out at room temperature,  $50^\circ\text{C}$ ,  $60^\circ\text{C}$  and  $90^\circ\text{C}$  using  $2.0 \mu\text{L}$  Pt precursor, Fig. 7. The results show that the particle size was maintained at  $\sim 2 \text{ nm}$ , independent of temperature, and there was no noticeable effect on the quantity of platinum decorated on CNOs. This data establishes that room temperature generates the optimum results, which has the lower energy requirements.

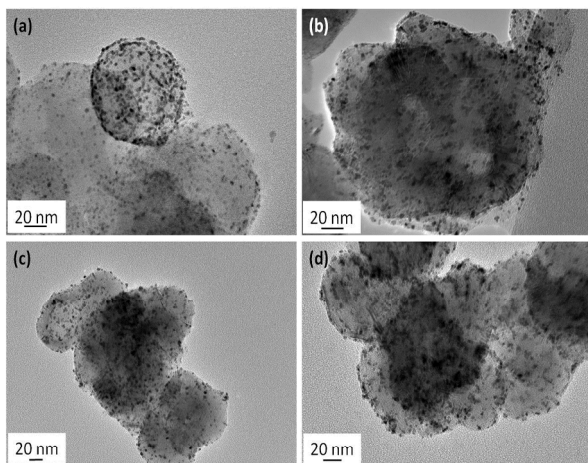


**Fig. 7.** TEM images of Pt@CNOs decorated at (a) room temperature, (b)  $50^\circ\text{C}$ , (c)  $60^\circ\text{C}$  and (d)  $90^\circ\text{C}$ .

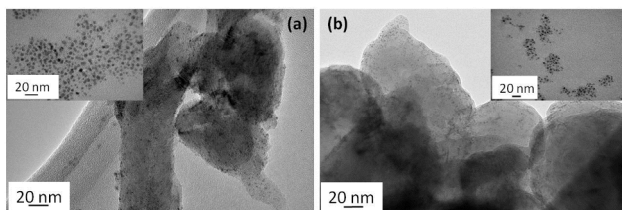


**Fig. 8.** TEM images of Pt decorated on plasma-etched CNOs with the amount of (a)  $2 \mu\text{L}$  and (b)  $5 \mu\text{L}$  Pt precursor. The inset images are the free-standing Pt nanoparticles in the two samples.

As mentioned earlier, the in situ functionalization of the CNOs is a benefit of this process, as non-functionalized graphitic substrates tend to result in the agglomeration of metal nanoparticles in large clusters. This is largely due to the complexity of dispersing metal nanoparticles uniformly on an inert surface.<sup>14</sup> Although the acid-treated CNOs already possess

charged sites, in order to identify if further sites would enhance the Pt-NP distribution, further pre-treatment was done using plasma etching in ambient air. As shown in Fig. 8, the use of plasma etching after the acid treatment had no obvious effect in improving the particle size and distribution of the Pt nanoparticles decorated on the CNOs. Furthermore, plasma-etched CNOs tended to result in free-standing Pt nanoparticles, with a lower density of CNOs decoration. It appears that the extra surface modification involved in the plasma etching promoted inter-growth of free standing metal particles over particles on the surface of CNOs.<sup>3</sup>

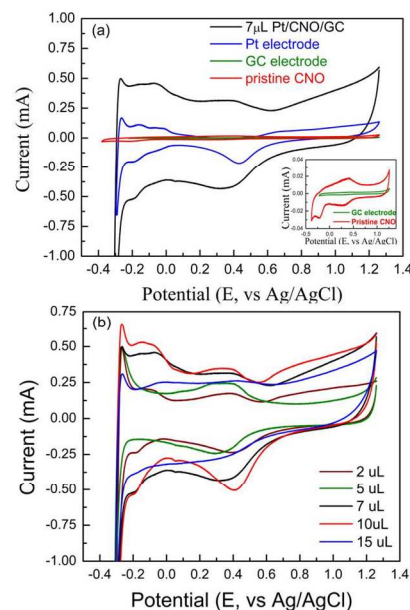


**Fig. 9.** Cyclic voltammograms of CNOs decorated with Pt nanoparticles in  $1.0 \text{ M H}_2\text{SO}_4$  at a scan rate of  $200 \text{ mV/s}$  for (a) the glassy carbon electrode, purified CNOs, pure Pt, and Pt@CNOs with  $7 \mu\text{L H}_2\text{PtCl}_6$ , and (b) CNOs decorated with different amount of  $\text{H}_2\text{PtCl}_6$  precursor.

Cyclic voltammetry (CV) in  $0.1 \text{ M H}_2\text{SO}_4$  solution was used to evaluate the electrocatalytic potential of Pt-decorated CNOs generated using various concentrations of the platinum precursor. While CV has been commonly used to evaluate the electrochemical activity of Pt/C materials as a catalyst for fuel cells,<sup>15</sup> there has been little emphasis on CNOs-based material. CNO, as a highly graphitic material, is an attractive support due to its high electrical conductivity, large surface area, and exceptionally fast charge-discharge rates.<sup>6</sup> Herein, all Pt-decorated CNOs had significantly greater redox activity than the blank glassy carbon (GC) electrode, Fig. 9. The inset in Fig. 9a shows that the acid-treated CNOs display Faradaic peaks at  $0.4 \text{ V}$  and of  $-0.2 \text{ V}$  vs  $\text{Ag/AgCl}$ . This Faradaic current can be ascribed to the surface groups introduced during the oxidative acid treatment.<sup>16</sup> Close to identical CV curves have been observed in acid-treated CNTs.<sup>16b</sup> The acid treatment in general introduces defect sites on the CNO surface, thereby increasing the edge plane-like structure which has been suggested to

increase oxygen reduction reaction (ORR) activity. According to the literature, CNTs with a greater percentage of edge planes have increased electrocatalytic activity over CNTs with a greater percentage of basal planes.<sup>16</sup> Therefore the introduction of more defects and hence edge planes into the surface of CNOs may enhance electrocatalytic activity.

As shown in Fig. 9a, the Pt-decorated CNOs exhibit the characteristic hydrogen adsorption/desorption and reversible oxidation peaks of Pt. The change in electrocatalytic potential of the various Pt-decorated CNOs formed from different concentrations of H<sub>2</sub>PtCl<sub>6</sub> can be seen in Fig. 9b. The hydrogen adsorption/desorption and platinum oxidation peaks increased in intensity with increased concentration of the Pt precursor added from 2.0 to 7.0 μL, due to the increased density of Pt nanoparticles on CNOs. The increasing trend ends at the 10 μL sample, which had a similar peak intensity to the 7 μL sample and reverses at 15 μL sample where the peak intensity decreased. This can be explained by the agglomeration of the Pt nanoparticles as highlighted in Fig. 6, thereby leading to a decrease in the Pt surface area.

## Conclusions

We have demonstrated a facile and scalable batch method to decorate Pt nanoparticles on CNOs without the need for any surface modification and special high-speed device. The method allows for aqueous processing and control over nanoparticle decoration density. We have established that CNOs enjoy a more uniform distribution and highest density of Pt nanoparticles with 40-100 wt% Pt loading. Furthermore, the Pt-decorated CNO composites show promising electrocatalytic activity and the CNOs can be produced cost effectively using a large-scale methane cracking method. These advantages may translate to the use of the composite material in PEM fuel cells and other electrochemical applications, with an inherent economic advantage. The full potential of CNO as electrochemical power sources still needs to be investigated, and the future is very promising.

## Acknowledgements

The authors would like to thank the Perth Mint and the Australian Research Council (ARC), and the Government of South Australia for funding the project. The authors acknowledge the facilities, and the scientific and technical assistance of the Australian Microscopy and Microanalysis Research Facility (AMMRF) at the school of Chemical and Physical Sciences, Flinders University and the AAMRF facility at the Centre for Microscopy, Characterization and Analysis, The University of Western Australia, a facility funded by the University, State and Commonwealth Governments. The authors also gratefully acknowledge the UWA spin out company Hazer Pty Ltd for access to and supply of the carbon nano-onions.

## Notes and references

- <sup>a</sup>School of Mechanical and Chemical Engineering, The University of Western Australia, 35 Stirling Hwy, Perth, WA 6009, Australia.  
Email : huitong.chua@uwa.edu.au
- <sup>b</sup>Centre for Strategic Nano-Fabrication, School of Biomedical, Biomolecular and Chemical Sciences, The University of Western Australia, WA 6009, Australia
- <sup>c</sup>Centre for NanoScale Science and technology, School of Chemical and Physical Sciences, Flinders University, Bedford Park, SA 5042, Australia
- <sup>d</sup>Surface Science & Technology Group, School of Chemistry, The University of Melbourne, VIC 3010, Australia
- 1 J. Xie, N. Zhang and V.K. Varadan, *Smart Mater. Struct.*, 2006, **15**, S5.
  - 2 K. Lee, J. Zhang, H. Wang and D.P. Wilkinson, *J. Appl. Electrochem.*, 2006, **36**, 507.
  - 3 X.J. Chen, W. Zang, K. Vimalanathan, K.S. Iyer and C.L. Raston, *Chem. Commun.*, 2013, **49**, 1160.
  - 4 Y. Si and E.T. Samulski, *Chem. Mater.*, 2008, **20**, 6792.
  - 5 (a) D. He, K. Cheng, T. Peng, M. Pan and S. Mu, *J. Mater. Chem. A*, 2013, **1**, 2126. (b) R.V. Hull, L. Li, Y. Xing, and C.C. Chusuei, *Chem. Mater.*, 2006, **18**, 1780.
  - 6 (a) D. Pech, M. Brunet, H. Durou, P. Huang, V. Mochalin, Y. Gogotsi, P.L. Taberna and P. Simon, *Nature Nanotech.*, 2010, **5**, 651. (b) M.E. Plonska-Brzezinska and L. Echegoyen, *J. Mater. Chem., A*, 2013, **1**, 13703.
  - 7 (a) X. Wang, Z. Tan, M. Zeng and J. Wang, *Scientific Reports*, 2014, **4**:4437. (b) F.D. Han, B. Yao and Y.J. Bai, *J. Phys. Chem. C*, 2011, **115**, 8923. (c) D. Pech, M. Brunet, H. Durou, P. Huang, V. Mochalin, Y. Gogotsi, P.L. Taberna and P. Simon, *Nature Nanotech.*, 2010, **5**, 651.
  - 8 A. Cornejo, W. Zhang, L. Gao, R.R. Varsani, M. Saunders, K.S. Iyer, C.L. Raston and H.T. Chua, *Chem. Eur. J.*, 2011, **17**, 9188.
  - 9 (a) F.M. Yasin, R.A. Boulos, B.Y. Hong, A. Cornejo, K. S. Iyer, L. Gao, H. T. Chua and C.L. Raston, *Chem. Commun.*, 2012, **48**, 10102. (b) Y. Goh, X.J. Chen, F.M. Yasin, P.K. Eggers, R.A. Boulos, X.L. Wang, H.T. Chua and C.L. Raston, *Chem. Commun.*, 2013, **49**, 5171. (c) X.J. Chen, F.M. Yasin, P.K. Eggers, Ramiz A. Boulos, X.F. Duan, R.N. Lamb, K.S. Iyer and C.L. Raston, *RSC Adv.*, 2013, **3**, 3213. (d) L. Yasmin, X.J. Chen, K.A. Stubbs and C.L. Raston, *Scientific Reports*, 2013, **3**:2282.
  - 10 (a) D. Roy, M. Chhowalla, H. Wang, N. Sano, I Alexandrou, T.W. Clyne and G.A.J. Amaratunga, *Chem. Phys. Lett.*, 2003, **373**, 52. (b) M.E. Plonska-Brzezinska, A.T. Dubis, A. Lapinski, A. Villalta-Cerdas and L. Echegoyen, *Chem. Phys. Chem.*, 2011, **12**, 2659.
  - 11 S.K. Sonkar, M. Ghosh, M. Roy, A. Begum, S. Sarkar, *Mat. Chem. Express*, 2012, **2**, 105.
  - 12 R. Yu, L. Chen, Q. Liu, J. Lin, K.L. Tan, S.C. Ng, H.S.O. Chan, G.Q. Xu and T.S.A. Hor, *Chem. Mater.*, 1998, **10**, 718.
  - 13 (a) J.D. Qiu, G.C. Wang, R.P. Liang, X.H. Xia and H.W. Yu, *J. Phys. Chem. C*, 2011, **115**, 15639. (b) J. Guo, X. Wang and B. Xu, *Mater. Chem. Phys.*, 2009, **113**, 179. (c) C. Wang, M. Waje, X. Wang, J.M. Tang, R.C. Haddon and Y.S. Yan, *Nano Lett.*, 2004, **4**, 345.
  - 14 (a) B.C. Satishkumar, E.M. Vogl, A. Govindaraj and C.N.R. Rao, *J. Appl. Phys. D*, 1996, **29**, 3173. (b) Z. Liu, X. Lin, J.Y. Lee, W. Zhang, M. Han and L.M. Gan, *Langmuir*, 2002, **18**, 4054.
  - 15 (a) X.X. Wang, Z.H. Tan, M. Zeng and J.N. Wang, *Scientific Reports*, 2014, **4**:4437. (b) X.R. Ye, Y. Lin and C.M. Wai, *Chem. Comm.*, 2003, **5**, 642. (c) B. Seger and P.V. Kamat, *J. Phys. Chem. Lett.*, 2009, **113**, 7990. (d) S.D. Thompson, L.R. Jordan, A.K. Shukla and M. Forsyth, *J. Electroanal. Chem.*, 2001, **515**, 61. (e) S.D. Thompson, L.R. Jordan and M. Forsyth, *Electrochim. Acta*, 2001, **46**, 1657.
  - 16 (a) R. Kannan, U. Bipinlal, S. Kurungot and V.K. Pillai, *Phys. Chem. Chem. Phys.*, 2011, **13**, 10312. (b) J.H. Chen, W.Z. Li, D.Z. Wang, S.X. Yang, J.G. Wen and Z.F. Ren, *Carbon*, 2002, **40**, 1193.